Crystal structures of *Sulfolobus solfataricus* topoisomerase III reveal that its C-terminal novel zinc finger part is a unique decatenation domain

Hanqian Wang[1,+], Junhua Zhang[2,+], Xin Zheng[1], ZhenFeng Zhang[2], Zhiyong Zhang[3], Yuhui Dong[1,4], Li Huang[2,5,*] and Yong Gong[1,*]

1 Multi-discipline Center, Institute of High Energy Physics, Chinese Academy of Sciences, Beijing, 100049, China

2 State Key Laboratory of Microbial Resources, Institute of Microbiology, Chinese Academy of Sciences, Beijing, 100101, China

3 CAS Key Laboratory for Biomedical Effects of Nanomaterials and Nanosafety, CAS Key Laboratory of Nuclear Radiation and Nuclear Energy Technology, Institute of High Energy Physics, Chinese Academy of Sciences, Beijing, 100049, China

4 Beijing Synchrotron Radiation Facility, Institute of High Energy Physics, Chinese Academy of Sciences, Beijing, 100049, China

5 College of Life Sciences, University of Chinese Academy of Sciences, Beijing, 100049, China

*Corresponding authors

Yong Gong:

Fax: +86 10 88235257, Tel: +86 10 88235257, email: yonggong@ihep.ac.cn

Li Huang:

Fax: +86 10 64807429; Tel: +86 10 64807430, e-mail: huangl@sun.im.ac.cn

[+]These authors contributed equally to this work.

Abstract
DNA topoisomerases are essential enzymes for a variety of cellular processes involved in DNA transactions. Many of the mechanistic insights into type IA DNA topoisomerases have principally come from studies on the prokaryotes and eukaryotes. However, a structural understanding of type IA topoisomerases in the Archaeal is lacking. Here we report the crystal structures of full-length *Sulfolobus solfataricus* topoisomerase III (*Sso* topo III) both by itself and in complex with an 8-base single-stranded DNA fragment, which were determined at 2.1 Å and 2.5 Å, respectively. The structures show that, as a member of type IA topoisomerases, *Sso* topo III adopts a torus-like architecture consisting of a four-domain core region and a novel C-terminal zinc finger domain (domain V). Upon binding to ssDNA, *Sso* topo III undergoes dramatic conformational changes, similar to those of other type IA topoisomerases. Structural analyses and biochemical assays revealed that domain V is essential for the DNA decatenation activity of *Sso* topo III. These findings establish *Sso* topo III as an alternative prototype of type IA topoisomerases to further understand the loop-independent decatenation mechanism in the enzyme-bridged strand passage model.

The overall topological state of DNA in cells is altered by DNA topoisomerases. In all three domains of life, conserved DNA topoisomerases are essential for a wide variety of cellular molecular processes involved in DNA transactions, such as DNA replication, transcription, repair, recombination, and chromatin dynamics[1-4]. There are two types of topoisomerases[1]. Type I topoisomerases cut only one strand of DNA, pass one or two strands through the break, and are released as the break is religated. Type II topoisomerases cleave both strands of the DNA duplex and pass another double strand out through the break before resealing of the double strand break. Type I enzymes can be further classified into three different families, types IA, IB and IC, on the basis of temporary covalent intermediates formed (5' or 3' covalent intermediate)[5].

A conserved characteristic toroidal fold formed by four domains (I-IV) has been found in the structures of type IA enzymes[6-12]. The results of structural studies of type IA enzymes in combination with biochemical and single-molecule experimental data provide compelling evidence in support of the enzyme-bridged strand passage model[13-23]. According to this model, type IA topoisomerases nick one DNA strand, and remain attached to the two ends of the nick. That is, the enzyme is not only covalently attached to one end of the nick, but also noncovalently bound to the other end to generate a bridge through which the intact strand or the DNA duplex is passed. The following step is the resealing of the nick and the release of the enzyme. In this process, the OH group of the aromatic ring of the Tyr residue in the enzyme nucleophilically attacks the scissile phosphodiester bond, producing a transient 5' phosphotyrosine covalent bond.

Members of the type IA subfamily can be further divided into two

mechanistically distinct subclasses based on their biochemical specificity for substrates[2]. *Escherichia coli* topoisomerase I (EcTOP1) and topoisomerase III (EcTOP3) are the prototypes of these two subclasses of type IA enzymes. EcTOP3 catalyses the DNA decatenation more effectively than it does the relaxation of negatively supercoiled DNA, whereas the converse is true for EcTOP1[22, 24-27]. EcTOP3, but not EcTOP1, contains a unique loop located close to the central hole[28]. This loop, known as the decatenation loop, is essential for the decatenation activity of EcTOP3[23, 28].

Previous studies have suggested that topoisomerase III (hereafter referred to as *Sso* topo III) from *Sulfolobus solfataricus*, a hyperthermophilic archaeon with an optimal growth temperature of 75°C, is a member of the type IA topoisomerase family, and is more similar to EcTOP3 than to EcTOP1[29]. More recently, Bizard *et al.* provided convincing biochemical evidences that *Sso* topo III is a genuine decatenase that can efficiently unlink covalently closed catenanes at temperatures up to 90℃ in the absence of additional partners[30]. However, little is known about the structure of type IA topoisomerases (except for reverse gyrase) in the Archaea. The structural basis by which *Sso* topo III, in isolation, is able to function as a true decatenase remains unclear. Here, we have determined the crystal structure of full-length *Sso* topo III, both on its own and in a complex with an 8-base ssDNA fragment. Structural analyses of *Sso* topo III revealed that it adopts a classical elongated toroidal-like shape. Its four domains (I-IV) form the protein core, and a novel C-terminal zinc finger domain (domain V) is tethered to the core domain against domain II. Biochemical analyses showed that domain V is essential for the DNA decatenation activity of *Sso* topo III. These findings indicated that *Sso* topo III may serve as an alternative prototype for type IA topoisomerases whose decatenation mechanism differs from that of known prokaryotic and eukaryotic topoisomerases III.

Results

Overall structure of intact *Sso* topo III

To obtain crystals of *Sso* topo III, we expressed and purified sufficient quantities of the mutant enzyme (Y318F) in which the catalytic residue Tyr318 was replaced with Phe (Fig. 1a). The structure of the full-length enzyme was determined at 2.1 Å resolution using molecular replacement. The full-length enzymes formed an asymmetric unit comprising four *Sso* topo III molecules (molecules A, B, C, and D). The four molecules had essentially the same architecture, except that the region spanning residues 600–607 was disordered in molecules A and B. For convenience, molecule D was chosen as the basis for the following structural analyses.

Our crystallographic analysis of *Sso* topo III showed that it adopts a canonical toroidal-like elongated configuration with a large hole (Fig. 1b), which is shared by all known type 1A topoisomerases[31]. The enzyme-bridged

strand passage model proposes that the hole accommodates single or double-stranded DNA[32]. The overall structure of *Sso* topo III comprises four domains (I–IV) (residues 1–593), forming the enzymatic conserved core, and a novel carboxyl-terminal domain V (residues 593–668) (Figs 1a,b and Supplementary Fig. 1).

Domain I (residues 1–219) exhibits a topoisomerase–primase (TOPRIM) fold, which is found in type IA, IIA, and IIB topoisomerases, and in bacterial primases[2]. Within domain I, a disulphide bridge crosslinks Cys4 of a loop (residues 1–10) and Cys34 of an α/β fold consisting of six parallel β sheets sandwiched with four α helices (Fig. 1b and Supplementary Fig. 1). This connection results in tight packing of domain I and stabilize its architecture. In Domain II (residues 220–277, 407–474), the flexible loop between β13 and β14, which is rich in charged residues, protrudes into the centre of the toroid hole (Fig. 1b). A charged loop shows similar orientation in the structure of EcTOP1 and EcTOP3[6, 7]. The flexible loop is thought to play a role in the strand passage step. The hinge region (residues 219–224, 471–480) is composed of the two loops linking domain I and II, and II and IV, respectively (Fig. 2b). The hinge was thought to serve as the principal pivot point for opening and closing of the gate in the strand passage reaction[6, 10, 33].

Analyses of the structure of EcTOP3 as the prototypical member of the type IA subfamily, together with biochemical experimental data, have indicated that the positively charged loop (known as decatenation loop) on domain IV is critical for efficient decatenation activity (Fig. 2a)[7, 17, 28]. A recent report on *Sso* topo III provides strong biochemical evidence that *Sso* topo III is a true decatenase[30]. Surprisingly, the structural equivalent of the decatenation loop is absent from *Sso* topo III (Fig. 2a), suggesting that the decatenation mechanism of *Sso* topo III differs from that of EcTOP3.

A long loop (residues 594–616) leads from helix α18 of domain IV to domain V (residues 594–668), thus linking the core of the enzyme to domain V (Fig. 1b and Supplementary Fig. 1). Domain V attaches to the top of the topoisomerase (domain II) gate against the hinge region (Figs 1b,c). Three antiparallel α-helices, including helix α19 (residues 616–636), helix α20 (residues 640–649), and helix α21 (residues 655–666), are coiled around each other to constitute the bulk of domain V (Fig. 1b and Supplementary Fig. 1). Interestingly, four residues (Cys602, Cys605, Cys615 and His618) coordinate with a zinc atom to generate a novel zinc-binding motif (Fig. 1b and Supplementary Fig. 1). Among them, the three Cys residues come from the long loop connecting domains IV/V and the His residue is from helix α19. The presence of the znic-binding site was confirmed by an analysis of the anomalous difference Fourier map (Fig. 1b). The recently characterized mesophilic archaeal topoisomerase, *Methanosarcina acetivorans* topo IIIα (*Mac* topo IIIα), also has one znic-binding site[34]. However, the zinc-binding motif of *Sso* topo III is the Cys_3His_1 type, whereas that of *Mac* topo IIIα is tetraCys type. Obviously, the zinc finger motif contributes to the stabilization of

domain V. Alignment of C-terminal sequences of of various topoisomerases occurring in the Crenarchaeota showed that, within domain V, the four residues comprising the zinc finger motif are fully conserved (Supplementary Fig. 2a), suggesting that this motif plays an important role. No structural element similar to domain V of *Sso* topo III was found in the Protein Data Bank, as detected by DALI[35]. This result suggested that the C-terminal fold of *Sso* topo III is unique.

Overall structure of *Sso* topo III in complex with ssDNA

To explore the structural mechanism of *Sso* topo III, co-crystals were obtained of the *Sso* topo III mutant (Y318F) in complex with an eight-base ssDNA molecule. The DNA sequence used for co-crystallization (5'-GCAAGGT ↓ C- 3', where the arrow indicates the preferred cleavage site) harbours an asymmetric cleavage site recognized by *Sso* topo III. The structure of the complex was determined at 2.5 Å by the single-wavelength anomalous dispersion (SAD) phasing method, using the peak wavelength of the zinc ion of 1.26 Å. The asymmetric unit consisted of one *Sso* topo III complex molecule. As expected, *Sso* topo III in the presence of ssDNA maintained almost the same toroidal fold of type IA topoisomerases as an apo enzyme (Figs 3a,b). The enzyme interacted with all eight nucleotides of its DNA substrate via direct hydrogen bonds and electrostatic interactions (Supplementary Fig. 3).

By analogy to EcTOP3, the relative movements of domain I result in realignment of the cluster of critical acidic residues(Glu15, Asp112, Asp114 and Glu116) to induce the assembly of an active site (Fig. 3c). The aromatic phenyl ring of Phe 318 points directly to the phosphodiester backbone at a distance of 3.8 Å (Fig. 3c). Arg320, Glu308 and Lys16 form a network of ionic and hydrogen bond interactions to hold the 3' end of the oligonucleotide in place (Fig. 3c).

Structural comparison of *Sso* topo III in the presence and absence of ssDNA

Superposition of *Sso* topo III in the presence and absence of ssDNA generated a root mean square deviation (r.m.s.d) of 2.488 Å for all main chain atoms (residues 1–668), indicating that significant conformational changes occur upon binding to ssDNA (Supplementary Fig. 4a). Superposition of each individual domain in the apo form and in the complex structure gave rise to r.m.s.d values of 0.875 Å, 0.738 Å, 0.571 Å, 1.957 Å, and 0.785 Å for domains I, II, III, IV and V, respectively (Supplementary Fig. 4a). As expected, dramatic rearrangements within domain IV occur in order to accommodate the oligonucleotide molecule along the binding groove. Superposition of domain I revealed that when the enzyme binds to ssDNA, the rest of the protein except for domain I, swings away from domain I by about 9°(Supplementary Fig. 4b),

which is not as acute as the conformational change in EcTOP3 (～20°)[17]. According to the mechanism proposed on basis of the structural studies of bacterial type IA topoisomerases, two factors contribute to elicit the overall conformational change in the enzyme upon ssDNA binding[36]. In the case of *Sso* topo III, one factor is an interaction at the base of helix α6 leading from domain I into domain II. Residues Arg201, Val202, Gln203, located on the amino terminus of this helix, interacts with the phosphodiester backbone of the oligonucleotide to clamp the ssDNA (Supplementary Fig. 3). In the presence of ssDNA, a slight shift of this helix helps to trigger the dramatic conformational change of the enzyme. Another factor is helix α14 spanning residues 497–508. In the presence of ssDNA along the binding cleft, helix α14 arranges itself parallel to the phosphodiester backbone. Several conserved residues located within or around helix α14, such as Thr494, Thr497 and Arg508, contact the phosphate groups of the oligonucleotide to hold it in place.

Glu308 is critical for the relaxation activity of *Sso* topo III

Structural alignment of the three available type IA topoisomerases (*Sso* topo III, EcTOP1 and EcTOP3) in complex with ssDNA showed that although they all bind to ssDNA in a similar manner, but there are some small differences among them (Figs 4a,b). Most obviously, the acidic side chain of Glu308 in *Sso* topo III forms a hydrogen bond with the hydroxyl group of the 3' end of the oligonucleotide (Fig. 4b and Supplementary Fig. 3). In contrast, the side chain of the Glu in EcTOP1 and EcTOP3 contacts the phosphate group of the 3' end nucleotide of the ssDNA (Fig. 4b). In addition, the side chain of Glu308 forms a salt bridge with a guanidinium group of Arg320 in *Sso* topo III, whereas a Gln in place of the Glu forms hydrogen bonds with the side chain of a strictly conserved Arg in EcTOP1 and EcTOP3 (Fig. 4b). Interestingly, this feature of Glu308 in *Sso* topo III is shared by yeast and mammalian topoisomerases III (Fig. 4c), suggesting a conserved functional role of this residue in eukaryotic and archaeal type IA enzymes[10].

These structural observations raise the question as to whether mutation of Glu308 would affect the relaxation activity of *Sso* topo III. To answer the question, we created mutant E308Q in which Glu308 was replaced by Gln, and mutant E308A in which Glu308 was replaced by Ala (Supplementary Table 1). The two mutant enzymes were expressed, purified to homogeneity, and assayed for relaxation activity. Both the E308Q and E308A mutant enzymes had at least a 16-fold reduction in relaxation activity as compared with that of wild-type *Sso* topo III (Figs 4d and 5a), implying that the interaction between Glu308 and the hydroxyl group of the 3' end of the oligonucleotide is critical for relaxation activity.

Interface of domains II and IV

A distinguishing feature of the overall structure of Sso topo III compared with

the other available type IA topoisomerases is the presence of three helices in domain V located close to the hinge region of domain II (Fig. 1b). Two flexible loops, each about five residues long, link these three helices. This arrangement causes the three helices to pack against each other so that their movement is highly coordinated, but they maintain a degree of flexibility. Additionally, within the long linker loop (about 20 residues) connecting domains IV and V, there are three successive turns that maintain free space between the two domains. The novel zinc-binding motif is located on the carboxyl-end of the long loop, provides a certain degree of stability to the loop (Fig. 1b). By analogy to the other solved type IA topoisomerases, the interfaces between domain III and domains IV and I in *Sso* topo III are conserved and far-ranging[6]. However, the interface between domain II and V in *Sso* topo III is unique.

The longest of three helices in domain V, helix α19, acts as the major binding interface between domain II and V. The interface is mostly, but not exclusively, hydrophobic (Fig. 1c). Extensive hydrophobic interactions mainly occur between the alkyl chains of Leu219, Ile221, Leu223, Pro224 in the hinge region, which connects helix α6 of domain I with sheet β9 of domain II, and the side chains of Ala621, Leu625, Ala628, Leu631, Trp632 in helix α19 of domain V (Fig.1c). Moreover, the main chain amides of Gly654 and Lys655 in domain V form hydrophilic interactions with the backbone carbonyl groups of Phe220 and Asn218 in the hinge region, respectively, to further stabilize binding (Fig.1c). Most importantly, the main chain carbonyl group and side chain amide of Arg635 in the carboxyl-end of helix α19 in domain V form hydrogen bonds with the main chain amide of Ile250 at the amino-end of helix α7 and the carbonyl group of Pro224 at the amino-end of strand β9 in domain II, respectively (Fig.1c). Domain V and the main part of domain II are connected by a single interaction, that is, double hydrogen bonds involving Arg635. This may allow for independent and coordinated relative movements of domain V against domain II at different stages during catalysis. Alignment of sequences of topoisomerases from organisms in the Crenarchaeota showed that most of the above mentioned residues contributing to the interaction between domains II and V are highly conserved (Supplementary Fig. 2). This implies that the interaction between domain II and V may be essential for the function role of domain V of archaeal topoisomerases.

Truncation of domain V reduces the relaxation activity of *Sso* topo III

To explore the role of the novel domain V of *Sso* topo III in catalysis, a C-terminally truncated mutant lacking an intact domain V (597ΔC), was generated by mutagenesis (Supplementary Table 1), expressed and purified to homogeneity. To assess the ability of 597ΔC to relax negatively supercoiled DNA, the standard relaxation assay was performed. In the assay, the 597ΔC mutant was capable of relaxing negatively supercoiled DNA but show only 6.25% of the activity of the wild-type enzyme(Fig. 5a), implying that domain V

facilitates the process of relaxation catalysed by the entire *Sso* topo III enzyme. To determine whether the zinc-binding site is required for relaxation activity, the C602S/C605S/C615S/H618A mutant (CCCH/M) was generated by site-directed mutagenesis (Supplementary Table 1), overexpressed in bacteria and purified to homogeneity. In the DNA relaxation assay, the activity of the CCCH/M mutant was only slightly lower than that of the wild-type enzyme (Supplementary Fig. 5b). This result was similar to that obtained for TmTOP1, but differs from that obtained for EcTOP1, which was completely inactive in a DNA relaxation assay when the zinc ion was eleminated[37, 38].

At higher temperatures (above 85°C), *Sso* topo III can split the two complementary DNA chains into two separate single-chains. To investigate whether the truncation of intact domain V affects this activity, we extended the temperature range of the DNA relaxation assay to 95°C as described by Bizard et.al[30]. At 85°C and above, the wild-type *Sso* topo III gradually changed the negatively supercoiled DNA into the FI* and FI** forms (Supplementary Fig. 5c), consistent with its recently characterized activity[30]. However, compared with the wild-type, the 597ΔC mutant inefficiently unlinked DNA at several high temperatures (Supplementary Fig. 5c).

Domain V is essential for decatenation activity of *Sso* topo III

Unlike type II topoisomerases, type IA topoisomerases cleave a single strand and require the presence of a single-stranded DNA region, such as a bubble, or a nick in one of the DNA circles to decatenate DNA catenanes[14]. *Sso* topo III, as a member of type IA topoisomerases, decatenates two covalently closed circular DNAs at high temperature, i.e., *Sso* topo III is a decatenase[30]. This striking feature results from the formation of short single-stranded DNA regions at high temperature.

To precisely determine the role of the novel domain V of *Sso* topo III in decatenation activity, the 597ΔC mutant enzyme was subjected to decatenation assays using kinetoplast DNA (kDNA) as the substrate. kDNA is a naturally occurring gigantic catenane network containing several thousand DNA minicircles, some of which are nicked or gapped[39]. The fast-migrating bands corresponding to closed minicircles, were present when the wild-type enzymatic reactions were performed at very high temperatures (90 °C and above) (Fig. 5b). This result suggested that closed minicircles were released from the kDNA network by the activity of *Sso* topo III, because at 90 °C and above, *Sso* topo III is not able to relax supercoiled DNA, but is still able to decatenate DNA catenanes[30]. Therefore, the presence of closed minicircles at very high temperature was considered as a measure of the decatenation activity of *Sso* topo III. The bands corresponding to closed minicircles were almost undetectable in the reaction mix containing the 597ΔC mutant enzyme (Fig. 5b), suggesting that 597ΔC had no detectable decatenation activity at very high temperature. Hence, the loss of intact domain V abolished the decatenation activity of *Sso* topo III at very high temperature. Since domain V

was found to be necessary for the decatenation activity of *Sso* topo III, it is designated as the decatenation domain.

Discussion

Topoisomerases are found in all three living domains. Many of the mechanistic insights gained for type IA topoisomerases have principally come from structural studies on prokaryotes and eukaryotes[40]. However, a structural understanding of type IA topoisomerases (except for reverse gyrase) in the Archaeal remains elusive. In this work, we report the structures of *Sso* topo III, an archaeal type IA topoisomerase. The crystal structures of full-length *Sso* topo III mutant both by itself and in complex with an 8-base single-strand DNA (ssDNA) were determined at 2.1 Å and 2.5 Å resolution, respectively. The crystal structures provide the first view of this archaeal topoisomerase, which removes negative supercoils and decatenates DNA catenane. *Sso* topo III is toroidal in shape with a four-domain protein core that closely parallels those found in other member of the topoisomerase IA family. A striking feature of *Sso* topo III is its C-terminal novel zinc finger-containing part that attaches to the hinge region of domain II. The C-terminal part (domain V) is required for effective decatenation and therefore is the decatenation domain of *Sso* topo III. Our work indicated that *Sso* topo III may be another promising experimental model to elucidate this decatenation mechanism which differs from those of the known prokaryotic and eukaryotic topoisomerases III.

The C-terminal domains of members of the type IA topoisomerase family vary widely in the composition and length of their primary sequence and in their shape[40, 41]. Despite these wide variations, they have ssDNA-binding activity, and play an important role in the high DNA-binding affinity of their corresponding enzymes. Our three-dimensional structures of Sso topo III provide the first molecular view of the C-terminal domain of type IA topoisomerases in the Archaea. The C-terminal domain of *Sso* topo III is unique, and harbours a zinc-binding motif (3Cys1His type) that differs from the tetracysteine zinc-binding motif conserved in prokaryotic type IA topoisomerases such as EcTOP1[42]. A structural analysis of the EcTOP1-DNA complex demonstrated that a zinc ribbon domain or zinc ribbon-like domain, mainly consisting of β-sheets, is solely capable of binding ssDNA, implying that these domains may not bind double-stranded DNA[42]. In some enzymes involved in DNA transactions such as transcription, replication and repair, the zinc-finger (ZF) domains, containing α-helixes, can bind to double-stranded DNA[43]. In the future studies, it will be very interesting to determine whether the C-terminal fold of Sso topo III has the capacity to bind double-stranded DNA. The first solved structure of a type IA topoisomerase indicated that domains II and III, as the rigid body, move away from domains I and IV in the strand passage reaction[6]. Further evidence for this movement has been provided by biochemical, structural data and single-molecule experiments[16-18, 20, 21, 23]. The hinge region joining domains II and IV presumably serves as a pivot point to

initiate the opening of the gate and possibly promote its closing[6, 10, 12]. In *Sso* topo III, major contacts between the hinge region and the longer helix α19 of domain V occur through extensive hydrophobic interactions. This arrangement may allow domain V to glide by the α19 helix along the hinge region up and down at some points during the strand passage reaction (Fig. 2b).

The extensive studies by structural and biochemical methods in combination with molecular dynamics simulations and single-molecule assays revealed that the decatenation activity of EcTOP3 is mainly caused by the interaction between the decatenation loop and the acidic loop, both of which line the central hole of the topoisomerase, during its gate dynamics[7, 17, 23, 28, 44] (Fig. 2a). The interaction in EcTOP3 presumably stabilizes and holds the open state for longer, thus allowing sufficient time for EcTOP3 to catch duplex DNA and pass it through the break in a single strand into the gate[23]. In the eukaryotic Top3a-RMI complex, RMI1 coordinates the gate dynamics of Top3a through its unique decatenation loop, which has a functionally equivalent role to that of the decatenation loop in EcTOP3[10]. Hence, a unified loop-mediated decatenation mechanism for prokaryotic and eukaryotic topoisomerases III has been proposed[10]. Our results demonstrated that domain V is essential for the DNA decatenation activity of *Sso* topo III. We provide the following evidence that the decatenation mechanism of *Sso* topo III is distinct from the unified loop-mediated decatenation mechanism presented for the type IA family: (i) The decatenation domain (domain V) of *Sso* topo III is a novel zinc finger part, whereas the decatenation loop is present in domain IV of EcTOP3. (ii) The decatenation domain of *Sso* topo III is on the outer edge of the topoisomerase gate, but attaches to domain II through the hinge region by extensive hydrophobic interactions, whereas the decatenation loop in EcTOP3 lines the gate and is separate from the hinge region of the catalytic core. (iii) The 597ΔC mutant enzyme lacking domain V showed an approximately 5-fold reduction in ssDNA-binding activity compared with wild-type *Sso* topo III (unpublished data). In contrast, the deletion of the decatenation loop from EcTOP3 did not reduce its ssDNA-binding activity. Further biochemical studies are needed to understand the molecular details of the unlinking of covalently closed catenanes catalszed by Sso topo III.

Methods

Gene Cloning, Protein Expression and Purification.

Using the standard PCR cloning strategy, the full-length topoisomerase III (hereafter, *Sso* topo III) gene from *S. solfataricus* genome was cloned into the NdeI and XhoI sites of the modified version of vector pET28a (Novagene), which harbored an N-terminal poly-histidine tag followed by a tobacco etch virus (TEV) protease cleavage site (ENLYFQ/G) (where '/' donates the cleavage site). However, the growth of *E.coli* cells harboring the wild type *Sso* topo III were severely inhibited, possibly due to its toxicity. So, *Sso* topo III

gene was mutated to the *Sso* topo III Y318F by replacing residue Tyr318 with Phe using the QuickChange Site-Directed Mutagenesis Kit (Stratagene) according to the instructions of manufacturer. The above constructs were confirmed by DNA sequencing.

The recombination *Sso* topo III Y318F was overexpressed as a fusion protein with an N-terminal poly-histidine tag in *E. coli* strain Rosetta2 (DE3) pLysS (Novagen). For each purification procedure, 10-l *E. coli* cultures harboring fusion proteins were grown in the shaker at 37℃ at 220 r.p.m. When their density reached an OD_{600nm} of 1.2, temperature of the cultures dropped to 25℃, followed by the addition of isopropylb-D-thiogalactoside (IPTG) to a final concentration of 0.5 mM. After growth for further 5 h at 25℃, the cultures were harvested, and the resulting cell sediments were suspended in solubilization buffer containing 20 mM Tris-HCl (pH 8.0), 2 mM $MgCl_2$, 20 mM imidazole and 500 mM NaCl supplemented with DNAaseI (55 μg/ml, Amersco), followed by disruption with a French press at 12,000 p.s.i. for three cycles. To remove cell debris, cell lysates were centrifuged for 40 min at 16,000 r.p.m. The resultant supernatant was collected and loaded onto an equilibrated Ni^{2+} Chelating Sepharose™ Fast Flow column (GE Healthcare). After several gradually crush washing, *Sso* topo III Y318F protein was eluted with a buffer containing 20 mM Tris-HCl (pH 8.0), and 500 mM NaCl supplemented with 300 mM imidazole. The eluate was digested using TEV protease to remove the poly-histidine tag, and dialyzed against a buffer containing 20 mM Tris-HCl (pH 7.5) and 150 mM NaCl overnight at 4°C. The eluate was filtered through a 0.45 μm filtration membrane prior to transfer into a 5 ml SOURCE 15S column (GE Healthcare). The *Sso* topo III Y318F was eluted with a linear NaCl gradient (0–100%) of elution buffer containing 20 mM Tris-HCl (pH 7.5), 1M NaCl, and 2 mM DTT. The purified homogenous protein fractions were pooled and concentrated to 8 mg ml^{-1} in a buffer containing 20 mM Tris-HCl (pH7.5), 150 mM NaCl, and 2 mM DTT for later usage. Purified protein was analyzed by sodium dodecy sulfate-polyacrylamide gel electrophoresis (SDS-PAGE) for purity and quantified with Bradford assay using BSA as standards. Typically 3 mg of *Sso* topo III Y318F protein can be purified from 10-l cultures.

Crystallization of Protein and Protein-DNA complex.

Sso topo III Y318F, both in isolation and in complex with ssDNA, was crystallized by the sitting-drop vapor diffusion method, with 0.7μl drops of protein or protein-ssDNA complex mixed with an equal volume of reservoir solution. For *Sso* topoisomerase III Y318F protein, initial crystallization trials screen clustered-needle-shaped crystals in reservoir solution containing 8% (v/v) Tacsimate (pH 4.4), and 20% (w/v) Polyethyleneglycerol 3,350. Further optimization of the crystallization condition led to the appearance of rod-shaped crystals in the well in which 0.7μl protein solution was mixed with an equal volume of reservoir solution consisting of 8% (v/v) Tacsimate (pH 4.4),

and 13.75% (w/v) Polyethyleneglycerol 3,350 at 12°C. The diffraction level crystals, by the microseeding method, appeared one week later and reached a maximum size within 2 months. These crystals in the mother liquor were exposed to air for 10 min, and transferred into a drop of paraffin and NVH mix oil before being crycooled by plunging rapidly in liquid nitrogen.

To assemble the complex of *Sso* topo III Y318F and ssDNA, the purified *Sso* topo III Y318F protein was mixed with the ssDNA (5'-GCAAGGTC-3') (Sangon Biotech) at a molar ratio of 1:1.2 for 30 min at 4℃. Crystals of the complex were grown from 0.7 μl drops of the complex solution and 0.7 μl of reservoir solution consisting of 0.1 M HEPES (pH 7.5), and 2.0 M ammonium sulfate at 20 ℃. The wedge-shaped crystals, by the microseeding method, grew from 0.7 μl drops of the complex solution mixed with an equal volume of reservoir solution consisting of 0.1 M HEPES (pH 6.6), and 2.25 M ammonium sulfate, and reached a maximum size within 5 days. These diffraction grade crystals were transferred to a cryoprotectant solution containing 1.5 M lithium sulfate prior to being flash-frozen in liquid nitrogen.

Crystallographic Data Collection, Structure determination and Refinement.

X-ray diffraction data of apo crystal were collected at the BL17U beamline of the Shanghai Synchrotron Radiation Facility (SSRF), and indexed, integrated and scaled using the HKL2000 package 1. The initial phases were determined by molecular replacement using the program PHASER 2， with the crystal structure of full length TOP1 from *Thermotoga maritima* (PDB ID: 2GAJ) as a searching model.

For the complex of *Sso* topo III Y318F and ssDNA, two X-ray diffraction data sets were collected at BL5A beamline of the Photon Factory (Japan): one data set was collected at the peak wavelength of zinc ion (1.26 Å) used for phasing through the single-wavelength anomalous dispersion (SAD) method, and the other done at the wavelength of 1.0 Å for refinement. These data sets were indexed, integrated and scaled using the HKL2000 package[45]. SAD phasing and density modification were performed using phenix.autosol[46] and phenix.autobuild from the PHENIX program suite[47].

The structure refinement was carried out with phenix.refine[48] and Refmac5[49]. Model building was carried out by iterative rounds of manual building with Coot[50]. MolProbity[51] was used to validate the structure. Data collection and refinement statistics are listed in Table 1.

All structural figures were rendered using PyMOL program (http://www.pymol.sourceforge.net/). For comparisons, the structures were superposed using the program LSQKAB of the CCP4 suite[52].

Assays of *Sso* topo III decatenation and relaxation activities.

DNA relaxation assay was performed as described previously with minor modifications. In briefly, The 20 ul standard reaction mixture (50 mM Tris, pH

8.8, 90 mM NaCl, 1 mM DTT, 0.1 mM EDTA, 30 ugml^{-1} BSA, 10 mM $MgCl_2$ and 12% (vol/vol) ethylene glycol) contained 300 ng of negatively supercoiled plasmid pUC18 DNA (www.thermofisher.com). The reactions were initiated by the addition various amounts of purified *Sso* topo III proteins, which were from serial dilution in a buffer containing 50 mM Tris, pH 8.0, 1 mM DTT, and 100 ug/ml BSA. After 30 min of incubation at 75°C unless indicated temperature otherwise, each reaction mix was added by 5 ul l of stopping buffer containing 100 mM EDTA, 2.5% SDS, 30% glycerol, 0.2% bromphenol blue, and 1 ug/ml Proteinase K (www.transgen.com.cn), and kept at 58°C for 30 min. Samples were electrophoresed through 1.4% agarose gel in TEP buffer (90 mM Tris-phosphate, pH 8.0, 2 mM EDTA) for 8 h at 2 V/cm. Gels were stained with 1 ugml^{-1} ethidium bromide and photographed under UV light.

Decatenation of kinetoplast DNA (kDNA) was carried out by a similar protocol except that 400 ng kDNA (www.topogen.com) was used as substrate in each standard reaction mixture. Reaction mixes were incubated at 90 °C for 30 min unless specified temperature otherwise, and the enzyme-catalysed products were examined by electrophoresis in 2% agarose gels.

Data availability.

Atomic coordinates and structure factors have been deposited in the PDB database under accession codes (apo) 6K8N and (binary complex) 6K8O.

All other data that support the findings of this study are available from the corresponding authors upon request.

References

1. Wang, J.C. DNA topoisomerases. *Annual review of biochemistry* **65**, 635-692 (1996).
2. Champoux, J.J. DNA topoisomerases: structure, function, and mechanism. *Annual review of biochemistry* **70**, 369-413 (2001).
3. Vos, S.M., Tretter, E.M., Schmidt, B.H. & Berger, J.M. All tangled up: how cells direct, manage and exploit topoisomerase function. *Nature reviews. Molecular cell biology* **12**, 827-841 (2011).
4. Pommier, Y., Sun, Y., Huang, S.N. & Nitiss, J.L. Roles of eukaryotic topoisomerases in transcription, replication and genomic stability. *Nature reviews. Molecular cell biology* **17**, 703-721 (2016).
5. Forterre, P. DNA topoisomerase V: a new fold of mysterious origin. *Trends in biotechnology* **24**, 245-247 (2006).
6. Lima, C.D., Wang, J.C. & Mondragon, A. Three-dimensional structure of the 67K N-terminal fragment of E. coli DNA topoisomerase I. *Nature* **367**, 138-146 (1994).
7. Mondragon, A. & DiGate, R. The structure of Escherichia coli DNA topoisomerase III. *Structure (London, England : 1993)* **7**, 1373-1383 (1999).

8. Rodriguez, A.C. & Stock, D. Crystal structure of reverse gyrase: insights into the positive supercoiling of DNA. *The EMBO journal* **21**, 418-426 (2002).
9. Hansen, G., Harrenga, A., Wieland, B., Schomburg, D. & Reinemer, P. Crystal structure of full length topoisomerase I from Thermotoga maritima. *Journal of molecular biology* **358**, 1328-1340 (2006).
10. Bocquet, N. *et al.* Structural and mechanistic insight into Holliday-junction dissolution by topoisomerase IIIalpha and RMI1. *Nature structural & molecular biology* **21**, 261-268 (2014).
11. Tan, K., Cao, N., Cheng, B., Joachimiak, A. & Tse-Dinh, Y.C. Insights from the Structure of Mycobacterium tuberculosis Topoisomerase I with a Novel Protein Fold. *Journal of molecular biology* **428**, 182-193 (2016).
12. Goto-Ito, S., Yamagata, A., Takahashi, T.S., Sato, Y. & Fukai, S. Structural basis of the interaction between Topoisomerase IIIbeta and the TDRD3 auxiliary factor. *Scientific reports* **7**, 42123 (2017).
13. Brown, P.O. & Cozzarelli, N.R. Catenation and knotting of duplex DNA by type 1 topoisomerases: a mechanistic parallel with type 2 topoisomerases. *Proceedings of the National Academy of Sciences of the United States of America* **78**, 843-847 (1981).
14. Kirkegaard, K. & Wang, J.C. Bacterial DNA topoisomerase I can relax positively supercoiled DNA containing a single-stranded loop. *Journal of molecular biology* **185**, 625-637 (1985).
15. Berger, J.M., Fass, D., Wang, J.C. & Harrison, S.C. Structural similarities between topoisomerases that cleave one or both DNA strands. *Proceedings of the National Academy of Sciences of the United States of America* **95**, 7876-7881 (1998).
16. Li, Z., Mondragon, A. & DiGate, R.J. The mechanism of type IA topoisomerase-mediated DNA topological transformations. *Molecular cell* **7**, 301-307 (2001).
17. Changela, A., DiGate, R.J. & Mondragon, A. Crystal structure of a complex of a type IA DNA topoisomerase with a single-stranded DNA molecule. *Nature* **411**, 1077-1081 (2001).
18. Zhang, Z., Cheng, B. & Tse-Dinh, Y.C. Crystal structure of a covalent intermediate in DNA cleavage and rejoining by Escherichia coli DNA topoisomerase I. *Proceedings of the National Academy of Sciences of the United States of America* **108**, 6939-6944 (2011).
19. Cejka, P., Plank, J.L., Dombrowski, C.C. & Kowalczykowski, S.C. Decatenation of DNA by the S. cerevisiae Sgs1-Top3-Rmi1 and RPA complex: a mechanism for disentangling chromosomes. *Molecular cell* **47**, 886-896 (2012).
20. Leelaram, M.N. *et al.* Type IA topoisomerase inhibition by clamp closure. *FASEB journal : official publication of the Federation of American Societies for Experimental Biology* **27**, 3030-3038 (2013).
21. Dekker, N.H. *et al.* The mechanism of type IA topoisomerases. *Proceedings of the National Academy of Sciences of the United States of America* **99**, 12126-12131 (2002).
22. Terekhova, K., Marko, J.F. & Mondragon, A. Single-molecule analysis uncovers the difference between the kinetics of DNA decatenation by bacterial topoisomerases I and III. *Nucleic acids research* **42**, 11657-11667 (2014).
23. Mills, M., Tse-Dinh, Y.C. & Neuman, K.C. Direct observation of topoisomerase IA gate dynamics. *Nature structural & molecular biology* **25**, 1111-1118 (2018).
24. Liu, L.F. & Wang, J.C. Interaction between DNA and Escherichia coli DNA topoisomerase I. Formation of complexes between the protein and superhelical and nonsuperhelical duplex DNAs. *The Journal of biological chemistry* **254**, 11082-11088 (1979).

25. Tse, Y. & Wang, J.C. E. coli and M. luteus DNA topoisomerase I can catalyze catenation of decatenation of double-stranded DNA rings. *Cell* **22**, 269-276 (1980).
26. DiGate, R.J. & Marians, K.J. Identification of a potent decatenating enzyme from Escherichia coli. *The Journal of biological chemistry* **263**, 13366-13373 (1988).
27. Terekhova, K., Gunn, K.H., Marko, J.F. & Mondragon, A. Bacterial topoisomerase I and topoisomerase III relax supercoiled DNA via distinct pathways. *Nucleic acids research* **40**, 10432-10440 (2012).
28. Li, Z., Mondragon, A., Hiasa, H., Marians, K.J. & DiGate, R.J. Identification of a unique domain essential for Escherichia coli DNA topoisomerase III-catalysed decatenation of replication intermediates. *Molecular microbiology* **35**, 888-895 (2000).
29. Dai, P., Wang, Y., Ye, R., Chen, L. & Huang, L. DNA topoisomerase III from the hyperthermophilic archaeon Sulfolobus solfataricus with specific DNA cleavage activity. *Journal of bacteriology* **185**, 5500-5507 (2003).
30. Bizard, A.H. *et al.* TopA, the Sulfolobus solfataricus topoisomerase III, is a decatenase. *Nucleic acids research* **46**, 861-872 (2018).
31. Capranico, G., Marinello, J. & Chillemi, G. Type I DNA Topoisomerases. *Journal of medicinal chemistry* **60**, 2169-2192 (2017).
32. Schoeffler, A.J. & Berger, J.M. DNA topoisomerases: harnessing and constraining energy to govern chromosome topology. *Quarterly reviews of biophysics* **41**, 41-101 (2008).
33. Feinberg, H., Lima, C.D. & Mondragon, A. Conformational changes in E. coli DNA topoisomerase I. *Nature structural biology* **6**, 918-922 (1999).
34. Morales, R., Sriratana, P., Zhang, J. & Cann, I.K. Methanosarcina acetivorans C2A topoisomerase IIIalpha, an archaeal enzyme with promiscuity in divalent cation dependence. *PloS one* **6**, e26903 (2011).
35. Holm, L. & Sander, C. Dali: a network tool for protein structure comparison. *Trends in biochemical sciences* **20**, 478-480 (1995).
36. Perry, K. & Mondragon, A. Structure of a complex between E. coli DNA topoisomerase I and single-stranded DNA. *Structure (London, England : 1993)* **11**, 1349-1358 (2003).
37. Tse-Dinh, Y.C. Zinc (II) coordination in Escherichia coli DNA topoisomerase I is required for cleavable complex formation with DNA. *The Journal of biological chemistry* **266**, 14317-14320 (1991).
38. Viard, T., Lamour, V., Duguet, M. & Bouthier de la Tour, C. Hyperthermophilic topoisomerase I from Thermotoga maritima. A very efficient enzyme that functions independently of zinc binding. *The Journal of biological chemistry* **276**, 46495-46503 (2001).
39. Englund, P.T. A passion for parasites. *The Journal of biological chemistry* **289**, 33712-33729 (2014).
40. Baker, N.M., Rajan, R. & Mondragon, A. Structural studies of type I topoisomerases. *Nucleic acids research* **37**, 693-701 (2009).
41. Viard, T. & de la Tour, C.B. Type IA topoisomerases: a simple puzzle? *Biochimie* **89**, 456-467 (2007).
42. Tan, K. *et al.* Structural basis for suppression of hypernegative DNA supercoiling by E. coli topoisomerase I. *Nucleic acids research* **43**, 11031-11046 (2015).
43. Krishna, S.S., Majumdar, I. & Grishin, N.V. Structural classification of zinc fingers: survey and summary. *Nucleic acids research* **31**, 532-550 (2003).

44. Xiong, B. *et al.* The type IA topoisomerase catalytic cycle: A normal mode analysis and molecular dynamics simulation. *Proteins* **71**, 1984-1994 (2008).
45. Otwinowski, Z. & Minor, W. Processing of X-ray diffraction data collected in oscillation mode. *Methods in enzymology* **276**, 307-326 (1997).
46. McCoy, A.J. *et al.* Phaser crystallographic software. *Journal of applied crystallography* **40**, 658-674 (2007).
47. Adams, P.D. *et al.* PHENIX: a comprehensive Python-based system for macromolecular structure solution. *Acta crystallographica. Section D, Biological crystallography* **66**, 213-221 (2010).
48. Afonine, P.V., Grosse-Kunstleve, R.W. & Adams, P.D. A robust bulk-solvent correction and anisotropic scaling procedure. *Acta crystallographica. Section D, Biological crystallography* **61**, 850-855 (2005).
49. Murshudov, G.N. *et al.* REFMAC5 for the refinement of macromolecular crystal structures. *Acta crystallographica. Section D, Biological crystallography* **67**, 355-367 (2011).
50. Emsley, P. & Cowtan, K. Coot: model-building tools for molecular graphics. *Acta crystallographica. Section D, Biological crystallography* **60**, 2126-2132 (2004).
51. Chen, V.B. *et al.* MolProbity: all-atom structure validation for macromolecular crystallography. *Acta crystallographica. Section D, Biological crystallography* **66**, 12-21 (2010).
52. Winn, M.D. *et al.* Overview of the CCP4 suite and current developments. *Acta crystallographica. Section D, Biological crystallography* **67**, 235-242 (2011).

Acknowledgments

We are grateful to Mei Li and Zengqiang Gao and the staff of beamline BL17U at the Shanghai Synchrotron Radiation Facility and the staff of beamline BL5A at the Photon Factory, KEK (Tsukuba, Japan) for technical support. This work was supported by the grants from the National Natural Science Foundation of China grant (No.U1432241) to Yong Gong and Zhiyong Zhang, and grants (No.31730001 and 30730003) to Li Huang. This work was also funded by the Strategic Priority Research Program of the Chinese Academy of Sciences (No. XDB08030103), the National Natural Science Foundation of China (No. 31570744) and the National Key Research and Development Project （No.2017YFA0504900）to Yuhui Dong.

Author contributions

Y.G., L.H., H.W. and J.Z. contributed to the design of this project. H.W., Y.G., X.Z., Z.Z. and Y.D. performed molecular cloning, protein purification, crystallization experiments, and collection of diffraction data, solution and analysis of the crystal structures. H.W., J.Z., Z.Z. and L.H. did functional assays. H.W., Y.G., J.Z., Z.Z., L.H. and X.Z. prepared and revised the manuscript of this publication.

Figures legends

Figure1. Overall structure of full-length *Sso* topo III.

A. Domain organization of *Sso* topo III. *Sso* topo III is composed of N-terminal four domains (domain I-IV) and the unique C-terminal domain V. Domains I-V are colored hotpink, green, cyan, orange, red, respectively.

B. Overview of *Sso* topo III. Domains I-V are colored in the legend to Fig. 1A. The close-up view (right) shows the anomalous difference electron density map (drawn in cyan mesh) around Zn (II) contoured at 15 σ using the diffraction data collected at the Zn absorption peak. The three Cys (C602, C605, C615) and one His residue (H618) coordinating Zn (II) are shown in sticks. Zn (II) is shown as a gray sphere.

C. Overview of *Sso* topo III. The close-up view (left) shows the interface between the domain II and V. The hydrogen bonds and hydrophobic contacts are made between residues originating from the loop linking helix α6 and sheet β9 and leading from helix α7, and residues originating from helices α19 and α21. Possible hydrogen bonds are drawn as dashed lines.

Figure 2. Comparison of structural element around the hinge region among *Sso* topo III, EcTOP1, EcTOP3, HsTop3α and HsTop3β.

A. Overall structural comparison among *Sso* topo III (hotpink), EcTOP3 (green) and HsTop3α (cyan). For clarity, the RMI1 subunit of HsTop3α complex (PDB entry 4CHT) is not shown. Domain V of *Sso* topo III is indicated. The decatenation loop and the acidic loop of EcTOP3 (PDB entry 1D6M) are shown, and their movement during the gate dynamics is shown with opposing arrows.

B. The close-up view around the hinge region of *Sso* topo III.

C. The close-up view around the hinge regions of HsTop3α in Top3α-RMI1

complex (PDB entry 4CHT), HsTop3β in Top3β-TDRD3 complex (PDB entry 5GVE) complexes, and EcTOP1. For clarity, the ssDNA molecule of EcTOP1 complex (PDB entry 4RUL) is not shown.

Figure 3. Overall structure of *Sso* topo III in complex with ssDNA.
A. Ribbon representations of the front and side views of the complex. Domains I–V of the enzyme are coloured hotpink, green, cyan, orange, and red respectively. The ssDNA molecule is shown in blues, e cartoon.
B. Surface representation of *Sso* topo III, revealing the deep groove where ssDNA (in green) binds.
C. The close-up views show that ssDNA induces the assembly of active sites of *Sso* topo III in comparison with apo enzyme. The active site of the apo structure is in close conformation, while the active site of the enzyme–ssDNA complex in open conformation. Residues in domain I and III, and bound DNA are shown as hotpink, cyan, and green sticks, respectively. Hydrogen bonds and salt bridges are depicted by black dotted lines.

Figure 4. Glu308 residue is required for the relaxation activity of *Sso* topo III.
A. Overall structural comparison of the available type IA topoisomerases in complex with ssDNA: *Sso* topo III in hotpink, EcTOP3 (PDB entry I17D) in cyan and EcTOP1 (PDB entry 3PX7) in green.
B. Close-up view of Glu residue or Gln residue contacting strictly conserved Arg residue and 3' end nucleotide of ssDNA in the same topoisomerases as Fig.4.A in stereo. Topoisomerases are colored in the legend as Fig.4.A. Oxygen atoms and nitrogen atoms are colored red and blue, respectively. For clarity, only the side chains of residues are shown.
C. Sequence alignment among six type IA topoisomerases including *Sso* topo III, EcTOP1, EcTOP3, TmTOP1 (from *Thermotoga maritima*), ScTOP3 (from *Saccharomyces cerevisiae*) and HsTOP3α (from *Homo sapiens*). Residues Glu (E) or Gln (Q), and Arg (R) are shown with black star and block below the alignment, respectively.
D. A representative relaxation experiment of E308Q and E308A mutant of *Sso* topo III. For each panel, pUC18 DNA was incubated at 75 °C for 30 min in relaxation buffer (50 mM Tris-HCl (pH 8.8), 10 mM MgCl2, 1 mM DTT, 0.1 mM EDTA, 90 mM sodium chloride, 30 μgml−1 BSA, and 12% (vol/vol) ethylene glycol)) with a titrated amount of either E308Q and E308A mutant (as indicated) including 500, 250, 64, 16, 4 and 1.0 ng, respectively. Reactions were terminated, the DNA products were separated in 1.4% agarose gels and visualized by staining with ethidium bromide. Oc indicates open circle nicked or gapped circular DNA; Sc denotes negatively supercoiled circular DNA; and Rel is the relaxed topoisomers.

Figure 5. Analysis of kinetoplast DNA (kDNA) and negatively supercoiled DNA

catalyzed by the wild-type *Sso* topo III and domain V-deleted mutant (597ΔC).

A. A representative relaxation experiment of 597ΔC mutant and the wild-type *Sso* topo III. DNA relaxation assays were performed as described in the legend to Fig.4D.

B. A comparison of kDNA decatenation activities of 597ΔC mutant and the wild-type enzyme. Decatenation assays were carried out as described for DNA relaxation assay except that kDNA (400 ng) was used as substrate with the amount of wild-type *Sso* topo III or 597ΔC mutant (as indicated) including 100 or 50 ng. The reactions were performed at the indicated three temperatures (85°C, 90°C, and 95°C) respectively and were terminated. Samples were electrophoresed through a 2% agarose gel, and the DNA products were visualized by staining with ethidium bromide. Lane CK corresponds to the kDNA control incubated at 90°C without the enzyme. Minicircles denote minicircle DNA released by *Sso* topo III.

Table 1. Data collection and refinement statistics

	Native *Sso* topo III	*Sso* topo III-ssDNA complex	
		Phasing Data Set	Refinement Data Set
Data collection			
Space group	$P2_1$	$P4_22_12$	$P4_22_12$
Cell dimensions			
a, b, c (Å)	110.7, 90.0, 156.2	150.8, 150.8, 97.0	150.7, 150.7, 97.0
α, β, γ (°)	90.0, 100.5, 90.0	90.0, 90.0, 90.0	90.0, 90.0, 90.0
Wavelength (Å)	0.9798	1.26	1.0
Resolution (Å)	50-2.10 (2.15-2.10) a	50-2.80 (2.85-2.80) a	50-2.50 (2.54-2.50) a
Rmerge	0.056 (1.316)	0.079 (1.045)	0.065 (0.882)
〈 I/σ(I)〉	24.3 (2.0)	65.0 (6.6)	21.7 (1.9)
Completeness (%)	96.4 (93.9)	100.0 (100.0)	99.9 (99.9)
Redundancy	7.0	57.0	7.6
Refinement			
Resolution (Å)	50-2.10		50-2.50

No. reflections	171,737	37,280
Rwork/ Rfree	0.203/0.247	0.220/0.259
No. atoms		
Protein	21,559	5,378
DNA	-	163
ZN	4	1
Water	1020	308
B-factors	46.4	49.1
Rmsd bond length (Å)	0.008	0.009
Rmsd bond angle (°)	1.2	1.2
Ramachandran Plot		
Favoured (%)	97.8	96.5
Allowed (%)	2.2	3.5
Outliers (%)	0.0	0.0

a The values in parenthesis mean those of the highest resolution shell.

Figure 1.

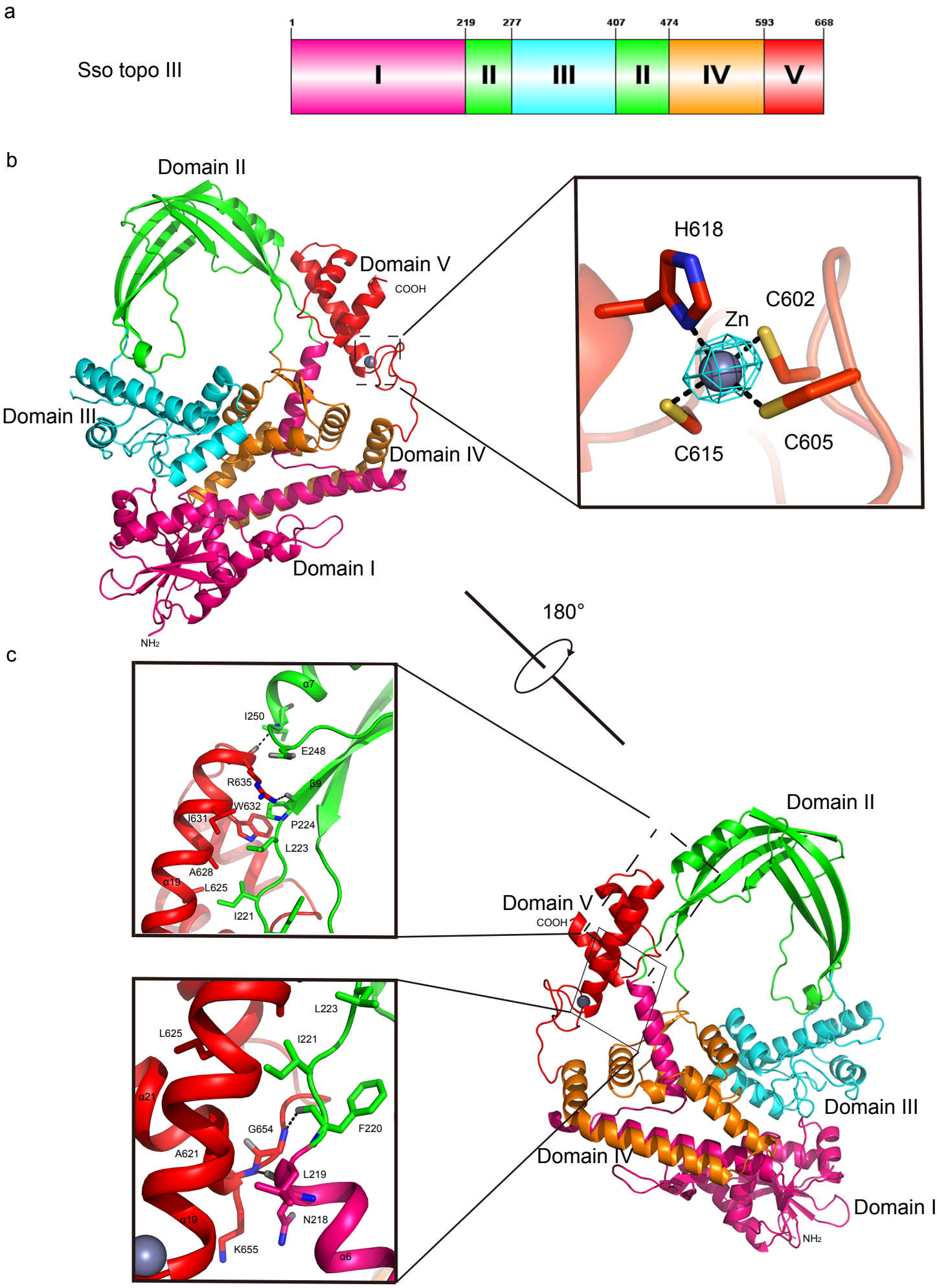
a
Sso topo III
1
219
277
407
474
593
668
I
II
III
II
IV
V
b
Domain II
Domain V
COOH
Domain III
Domain IV
Domain I
NH2
H618
C602
Zn
C615
C605
180°
c
α7
I250
E248
R635
β9
W632
I631
P224
L223
A628
α19
L625
I221
Domain II
Domain V
COOH
L223
L625
I221
α21
G654
F220
A621
L219
α19
N218
K655
α6
Domain III
Domain IV
Domain I
NH2

Figure 2.

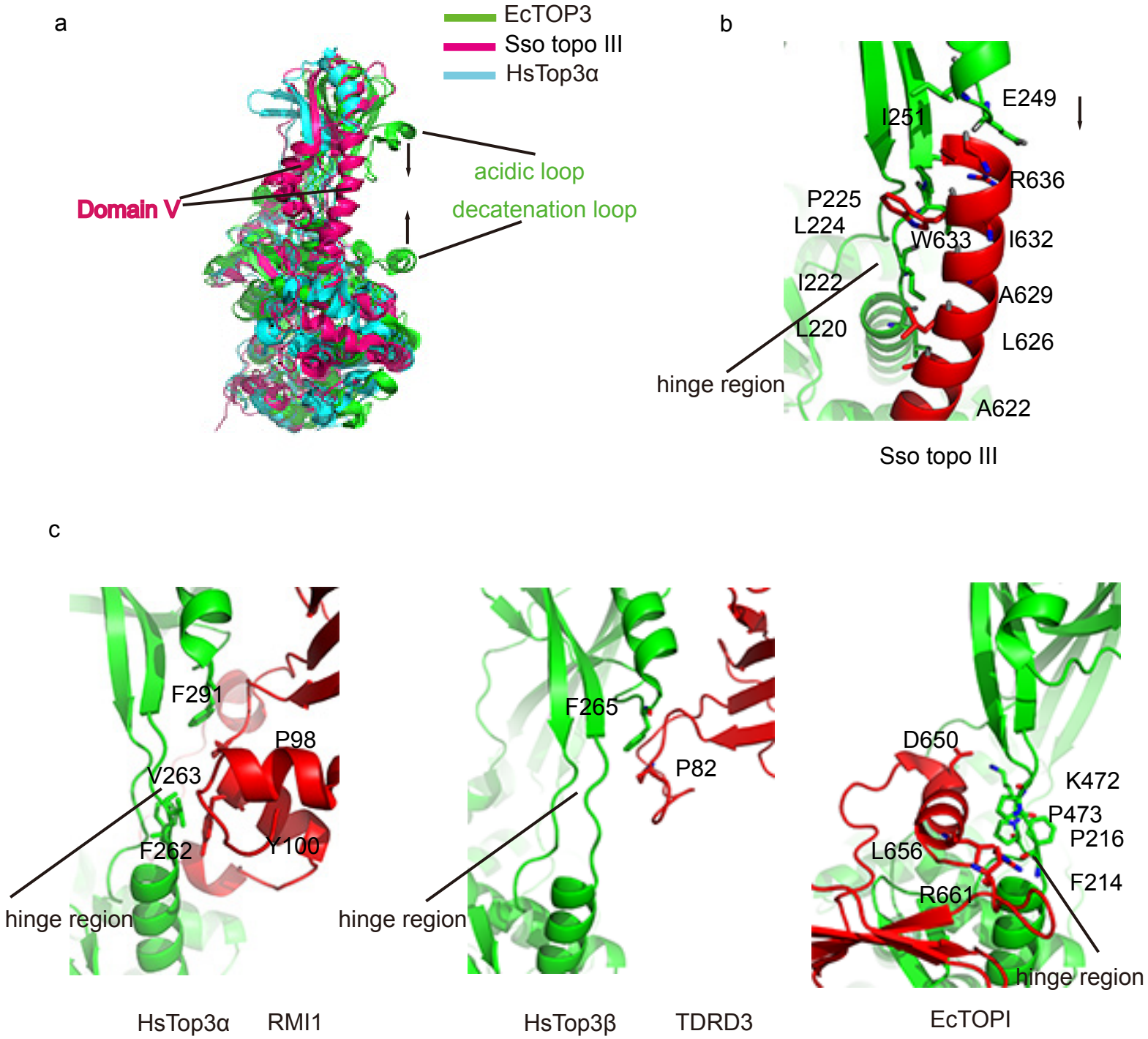
a
EcTOP3
Sso topo III
HsTop3α
Domain V
acidic loop
decatenation loop
b
E249
I251
R636
P225
L224
W633
I632
I222
A629
L220
L626
hinge region
A622
Sso topo III
c
F291
P98
V263
F262
Y100
hinge region
HsTop3α
RMI1
F265
P82
hinge region
HsTop3β
TDRD3
D650
K472
P473
P216
L656
F214
R661
hinge region
EcTOPI

Figure 3.

a

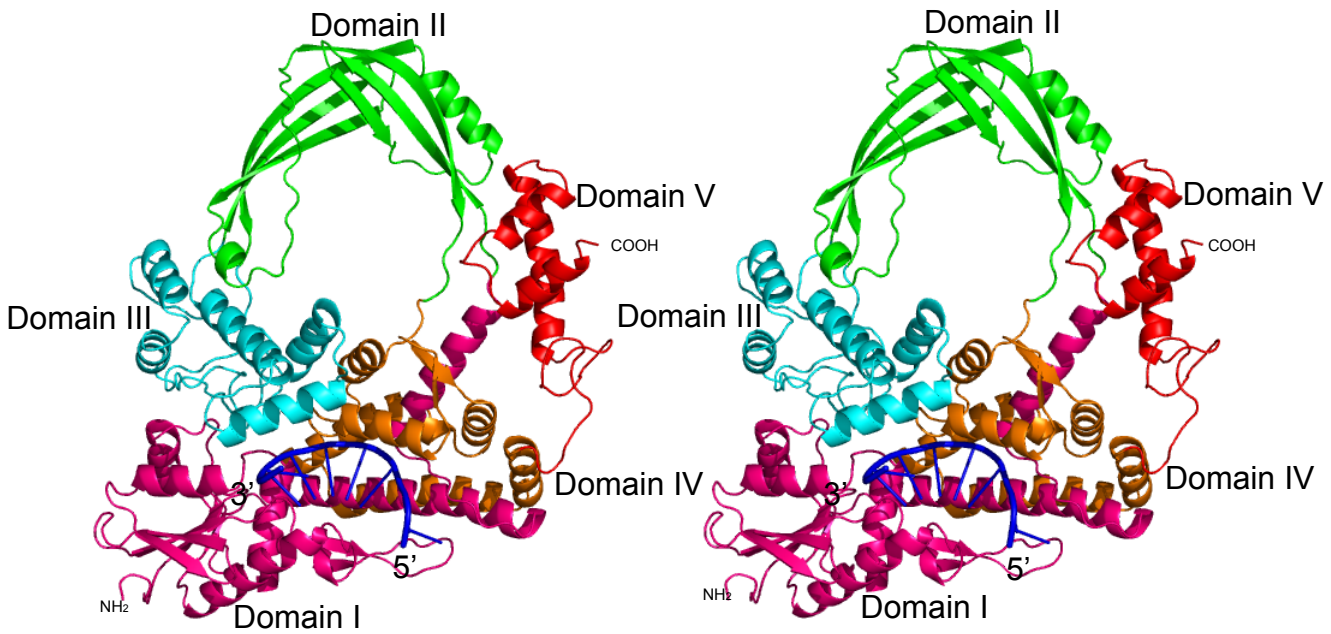

b

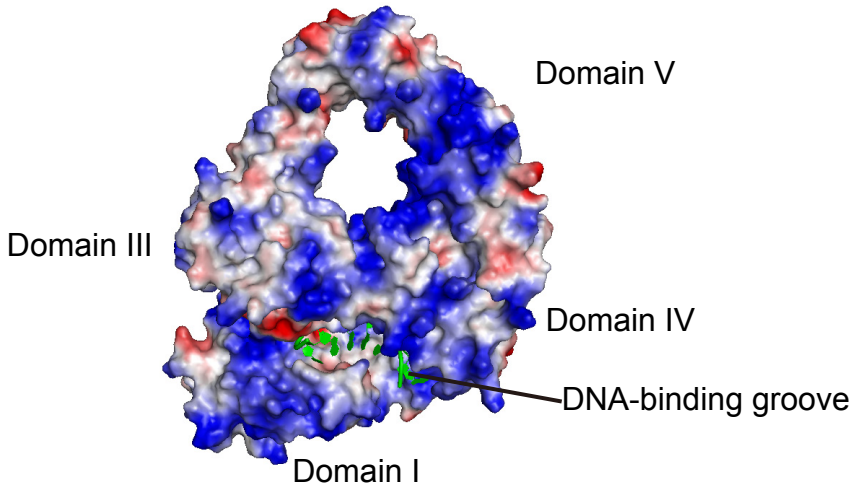

c

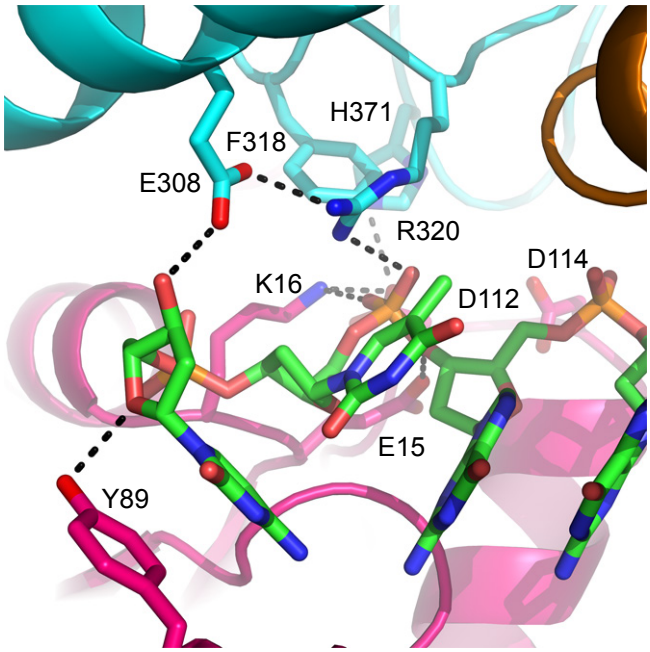

S. so topo III +DNA

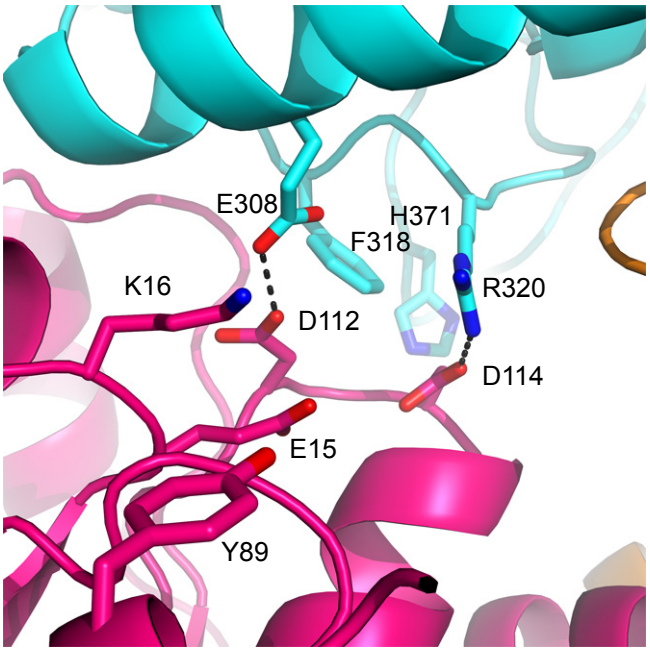

apo S. so topo III

Figure 4.

a

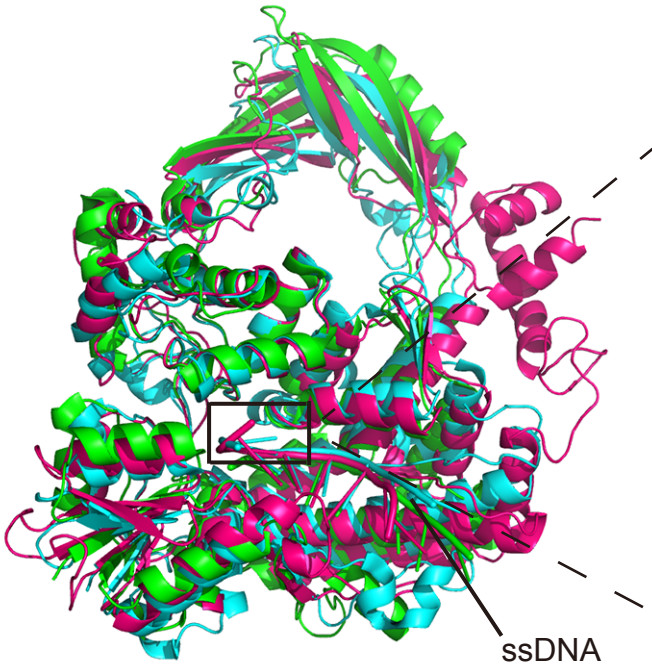

b

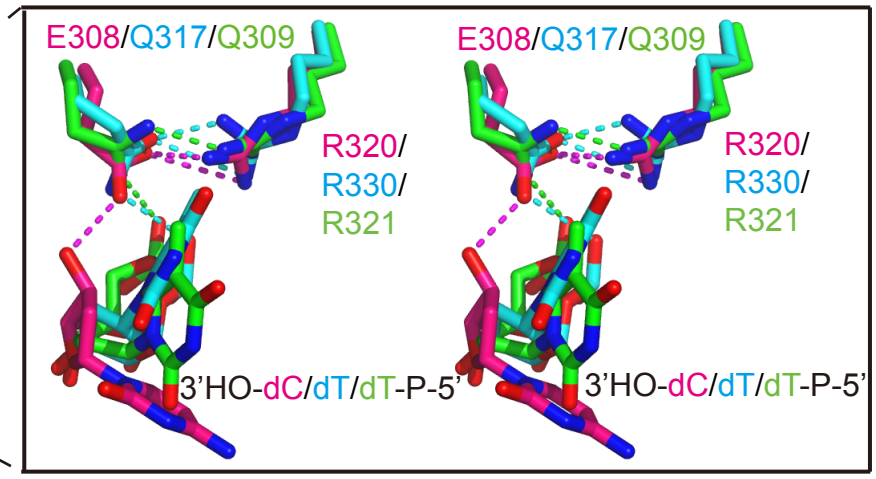

C

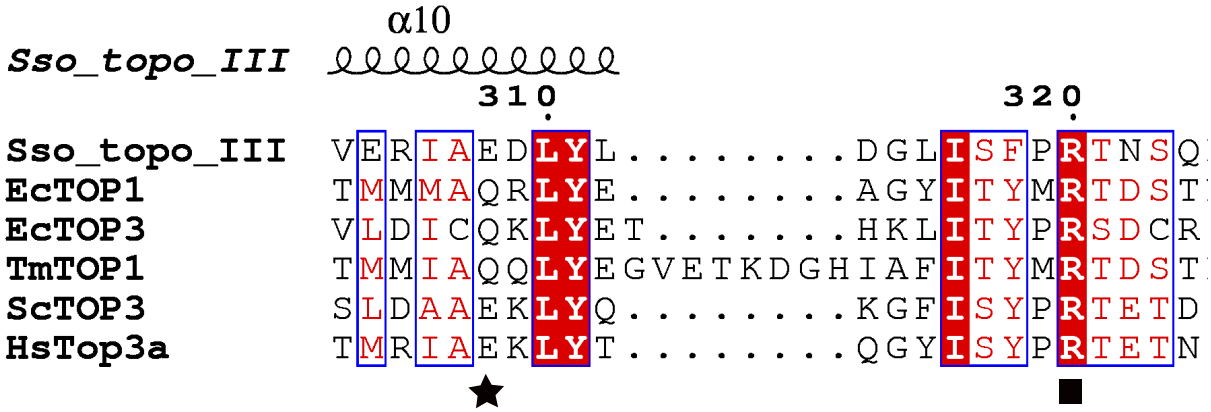

d

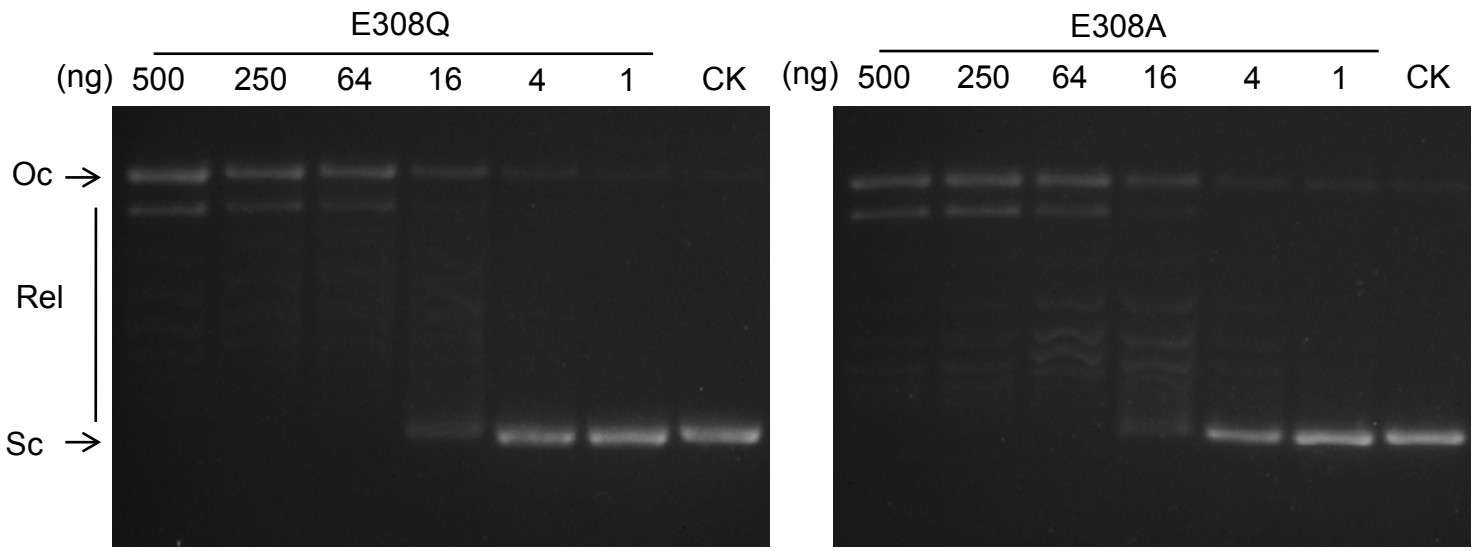

Figure 5.

a

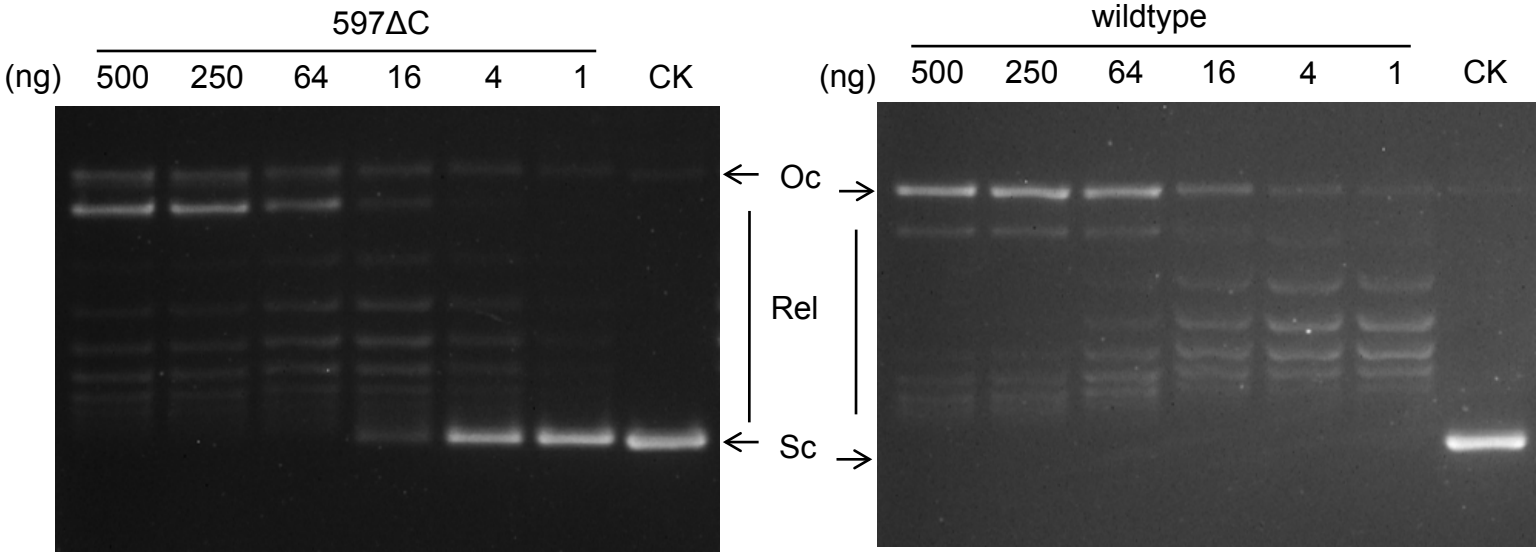
597ΔC
(ng) 500 250 64 16 4 1 CK
wildtype
(ng) 500 250 64 16 4 1 CK
Oc
Rel
Sc

b

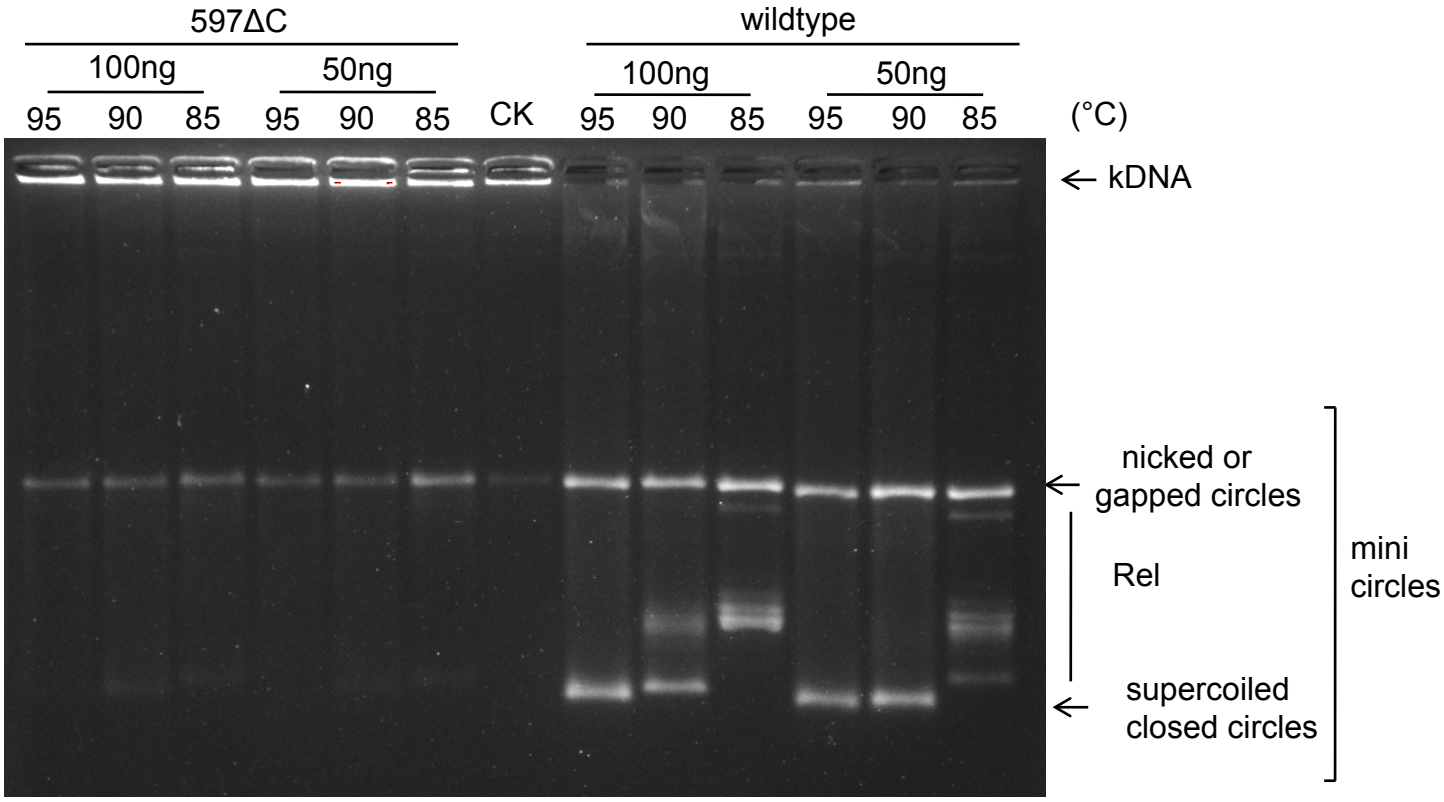
597ΔC
100ng
50ng
95 90 85 95 90 85 CK
wildtype
100ng
50ng
95 90 85 95 90 85
(°C)
kDNA
nicked or
gapped circles
Rel
supercoiled
closed circles
mini
circles